arXiv:astro-ph/0611029v2 22 Nov 2006

Scalar potential model of spiral galaxy H I rotation curves and rotation curve asymmetry

J.C. Hodge[1][*][†]
[1]Blue Ridge Community College, 100 College Dr., Flat Rock, NC, 28731-1690

February 5, 2008

Abstract

A scalar potential model (SPM) was developed from considerations of galaxy clusters and of redshift. The SPM is applied to H I rotation curves (RCs) and RC asymmetry of spiral galaxies. The resulting model adds the force of a scalar potential of the host galaxy and of neighboring galaxies to the Newtonian rotation velocity equation. The RC is partitioned radially into regions. The form of the equation for each parameter of each region is the same with differing proportionality constants. Integer values of each equation are determined empirically for each galaxy. Among the sample galaxies, the global properties of galaxies of B band luminosity, of position, and of orientation determine the RC and RC asymmetry. The Source of the scalar field acts as a monopole at distances of a few kpc from the center of spiral galaxies. The scalar potential field causes Newtonian mechanics to considerably underestimate the mass in galaxies, which is the "missing mass problem". The SPM is consistent with RC and RC asymmetry observations of the sample spiral galaxies.

Galaxies: kinematics and dynamics – Galaxies: fundamental parameters – Galaxies: interactions – Galaxies: spiral

1 Introduction

The discrepancy between the Newtonian estimated mass in spiral galaxies and the observation of star and gas kinematics is well established. The rotation curve (RC) relates the square of the tangential rotation velocity v (km s^{-1}) of particles in orbit around spiral galaxies to their galactocentric radius R (kpc). The RC is measured along the major axis. Traditionally, the focus has been on accounting for H I RCs that are flat in the outer region immediately beyond the knee (OR). However, observations also include rising RCs, declining RCs, an abrupt change in slope at the extreme outer region (EOR) in many galaxies, and rotational asymmetry with non-relativistic velocities. Battaner & Florido (2000); Ferrarese & Merritt (2002); Ghez et al. (2000); Sofue et al. (1999); Sofue & Rubin (2001); and Takamiya & Sofue (2000) provide a summary of the knowledge of RCs. The RC is an excellent tool to evaluate galaxy models.

The RC differs for different particles. For example, the H I RC and the RCs of stars as shown by the Hα line for NGC 4321 (Sempere et al., 1995) differ in the rapidly rising region before the knee (RR) and approach each other in the OR as shown in Fig. 1.

The stars near the center of galaxies have rotation velocities more than an order of magnitude larger than v at the knee of the H I RC. The decline of the

---

[*] E-mail:jch9496@blueridge.edu

[†] Visiting from XZD Corp., 16 Hosta Ln., Brevard, NC, 28712, E-mail:scjh@citcom.net

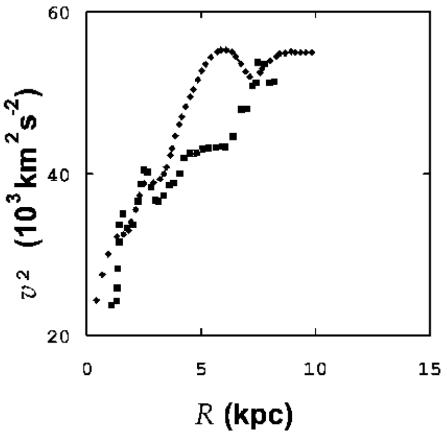

Figure 1: Plots of the square of the rotation velocity v^2 (10^3 km^2 s^{-2}) versus galactocentric radius R (kpc) of the H I RC (filled diamonds) and Hα RC (filled squares) for NGC4321 (Sempere et al., 1995).

stellar RCs from the center is Keplerian (Ghez et al., 2000; Ferrarese & Merritt, 2002). The v continues to decline to the radius R_Δ (kpc) at which the rotation velocity v_Δ is at a minimum. The v_Δ is approximately an order of magnitude smaller than v at the knee of the H I RC.

The H I RC rarely extends inward to near R_Δ. When drawing the H I RC, a straight line is often drawn from the innermost measured point through the center of the galaxy. This practice is inconsistent with stellar observations (Schödel et al., 2002) and is incorrect (Sofue & Rubin, 2001).

The evidence that the cluster environment affects RC shape appears contradictory (Whitmore et al., 1988; Dale et al., 2001). These studies concentrated on Hα RCs. The H I RC usually extends farther outward than Hα RCs. Therefore, the H I RCs are more sensitive to neighboring galaxy's effects.

As larger samples of RCs have been measured, researchers attempted to produce a quantitative description of an empirically derived, average RC. Persic et al. (1996) claimed the existence of a universal RC (URC) for a large sample revealed by the feature that only luminosity of the host galaxy dictated the RC. Independent work has confirmed much of the URC (Catinella et al., 2006, and references therein). Other researchers have discussed the inadequacy of the average RC (e.g. Courteau 1997; Garrido et al. 2004; Willick 1999).

Roscoe (2002) used a dynamical partitioning process and found that the dynamics in the outer part of optical RCs are constrained to occupy one of four *discrete dynamical classes*. The classes are determined by the absolute magnitude, surface brightness, and a parameter for each optical RC that is an exponent of the radius at which v is measured.

Galaxies with a small asymmetry in the RC of a few km s^{-1} are well known (Shane & Bieger-Smith, 1966). Large RC asymmetries are less appreciated (Jog, 2002). Because the observational data from each side of a galaxy RC are generally averaged, only highly asymmetric cases are recognized. RC asymmetry appears to be the norm rather than the exception (Jog, 2002). Weinberg (1995) and Jog (1997) proposed the implied mass asymmetry is due to an imposed lopsided potential caused by galaxy interaction. Dale et al. (2001) found RC asymmetry of early type galaxies falls by a factor of two between the inner and outer regions of clusters. The formation, evolution, and long term maintenance of galactic, kinematical asymmetry remains a mystery.

With the improved H I measuring equipment in the 1990's, the H I RC observations detected an abrupt change in the EOR in many galaxies (see figures in Catinella et al. 2006). This characteristic is ignored in current models. For example, Pizzella et al. (2005) considered this factor as a reason to exclude galaxies from the sample.

Spectra coming from HII regions are correlated systematically with R and little else (Binney & Merrifield, 1998, pp. 516-522). The interstellar abundances of metals in a disk galaxy decrease with increasing radius (Tadross, 2003). Also, the absolute B band magnitude M_{B} (mag.) of a galaxy is correlated with the metallicity obtained by extrapolating [O/H] within the disk to the galactic center. Low luminosity galaxies tend to be metal poorer than high luminosity galaxies.

If most of the matter of a galaxy is in the bulge region, classical Newtonian mechanics predicts a Keplerian declining RC in the disk. The observation of rising RCs in the RR and of rising, flat, or declining RC's in the OR poses a perplexing problem. Postulates to model the RCs have included the existence of a large mass M_{DM} of non-baryonic, dark matter (DM) and dark energy; the variation of the gravitational acceleration R; the variation of the gravitational constant G with R; and the existence of an added term to the Newtonian gravitation equation opposing gravitational attraction.

Repulsive DM has been proposed to provide a repulsive force that has the form of an ideal, relativistic gas (Goodman, 2000). In DM models the rising RCs of low surface brightness galaxies (LSBs) require larger relative amounts of DM than flat or declining RCs. This contradiction to the successful Tully-Fisher relation (TF) (Tully & Fisher, 1977) is well established (Sanders & McGaugh, 2002). Another mystery of the DM paradigm is the apparent strong luminous-to-dark matter coupling that is inferred from the study of RCs (Persic et al., 1996).

Currently, the most popular modified gravity model is the Modified Newtonian Dynamics (MOND) model (Bottema et al., 2002; Sanders & McGaugh, 2002, and references therein). MOND suggests gravitational acceleration changes with galactic distance scales by a fixed parameter related to the mass-to-luminosity ratio with units of acceleration. MOND appears limited to the disk region of spiral galaxies. MOND requires the distance for NGC 2841 and NGC 3198 to be considerably larger than the Cepheid-based distance D_{a} (Mpc) (Bottema et al., 2002). Appling MOND to cosmological scales is being investigated (Bekenstein, 2004; Sanders, 2006). MOND may represent a *effective* force law arising from a broader force law (McGaugh, 1999).

The possible variation of G or $|\dot{G}/G| \sim H_{\mathrm{o}}$, where H_{o} is the Hubble constant, were first proposed by Dirac. This was followed by the Brans-Dicke theory of gravity that postulated G behaves as the reciprocal of a scalar field whose source is all matter in the universe (Narlikar, 2002). More recently Brownstein & Moffat (2006, and references therein) have proposed a variation of general relativity in which G varies with R. This model has been applied to RCs (Brownstein & Moffat, 2006; Moffat, 2005) and the postulated gravitational radiation of binary pulsars. This model has results similar to the MOND model. However, it uses a distance D (Mpc) for NGC 2841 of 9.5 Mpc rather than D_{a} =14.07 Mpc (Macri et al., 2001).

Alternate models of the RC posit the existence of another term in the Newtonian equation resulting from a scalar field of a “fifth force”, a scalar field coupled to matter, or a static[1] scalar field coupled to DM. Padmanabhan & Choudhury (2002, and references therein) explored the possibility of a scalar field acting as dark matter. The usual “fifth force” models posit a Yukawa like potential (Bertolami & Páramos, 2005). Fay (2004) postulated minimally coupled and massive scalar fields are responsible for flat RCs, only. Mbelek (2004) suggested a real scalar field, minimally coupled to gravity sourced by baryonic and dark matter may also reproduce flat and rising RCs with the assumption that the dark halo mass density dominates the baryonic mass density. The free parameters are a turnover radius r_o, the maximum rotation velocity, which is at r_o, and an *integer*. If a natural theoretical explanation could be found for the relation between r_o and the positive integer, the integer may be the only free parameter. The postulate of an unknown "fifth force" is as likely as the postulate of unknown and undetected DM.

---

[1] Static in analogy to an electrostatic field caused by charged particles.

The scalar potential model (SPM) was created to be consistent with the observation of the morphology-radius relation of galaxies in clusters, of the intragalactic medium of a cluster of galaxies, and of the flow of matter from spiral galaxies to elliptical galaxies (Hodge, 2006). The SPM was applied to redshift observations and found a qualitative explanation of discrete redshift observations. The SPM suggests the existence of a massless scalar potential $\rho \propto R^{-1}$ derived from a heat differential equation. Physically, the heat equation requires a flow[2] of energy from Sources to Sinks to form the potential field. That the $\vec{\nabla}\rho$ field acts like a "wind" was suggested. Several differences among galaxy types suggest that Sources of ρ are located in spiral galaxies and that Sinks of ρ are located in elliptical, lenticular, and irregular galaxies. The Source forming a galaxy leads to the proportionally of the Source strength and emitted radiation (luminosity). Therefore, the total mass of a galaxy is related to the luminosity of a galaxy. A cell structure of galaxy groups and clusters was proposed with Sinks at the center and Sources in the outer shell of the cells. The cell model is supported by the data and analysis of Aaronson et al. (1982); Ceccarelli et al. (2005); Hudson et al. (2004); Lilje et al. (1986); and Rejkuba (2004). Because the distance between galaxies is larger than the diameter of a galaxy, the Sources were considered as point (monopole) Sources.

The force $\vec{F}_\mathrm{s}$ (dyne) of the ρ field that acts on matter is

$$\vec{F}_\mathrm{s} = G_\mathrm{s} m_\mathrm{s} \vec{\nabla}\rho \,, \tag{1}$$

where (1) the G_s is a proportionality constant; (2) m_s is the property of particles on which $\vec{F}_\mathrm{s}$ acts; and (3) ρ is the sum of the effects of all galaxies,

$$\rho = K_\epsilon \sum_{i=1}^{N_\mathrm{source}} \frac{\epsilon_i}{r_i} + K_\eta \sum_{l=1}^{N_\mathrm{sink}} \frac{\eta_l}{r_l} \,, \tag{2}$$

where ϵ_i and η_l are numbers representing the strength of the i^{th} Source and l^{th} Sink, respectively, K_ϵ and K_η are proportionality constants, and r_i (Mpc) and r_l (Mpc) are the distance from a Source and a Sink, respectively, to the point at which ρ is calculated, $\epsilon > 0$, $\eta < 0$, and N_source and N_sink are the number of Sources and Sinks, respectively, used in the calculation.

Hodge (2006) suggested the m_s property of matter is the cross section of the particle; the $\epsilon \propto M_{\mathrm{t}\epsilon}$, where $M_{\mathrm{t}\epsilon}$ is the total mass of the Source galaxy; and the $\eta \propto M_{\mathrm{t}\eta}$, where $M_{\mathrm{t}\eta}$ is the total mass of the Sink galaxy.

This Paper further constrains the SPM to describe another set of observations inconsistent with present models. The SPM finds the RC in the OR may be rising, flat, or declining depending on the galaxy and its environment. The Source of the scalar field acts as a monopole at distances of a few kpc from the center of spiral galaxies. In addition to fitting the RR and OR parameters, the SPM is consistent with EOR and asymmetry observations. In section 2, the model is discussed and the SPM v^2 calculation equation is developed. The resulting model is used to calculate RC parameters in Section 3. The discussion and conclusion are in Section 4.

---

[2] A flow of energy is in contrast to a static field. An analogy is the flow of gas or fluid from Sources to Sinks.

2 Spiral galaxy model

The coordinate system center was placed at the sample galaxy's kinematical center and was aligned to our line of sight. The SPM posits the simplified Newtonian calculation of v of a test particle is the first approximation of v in an isolated galaxy, that observed asymmetries and deviations from the simplified Newtonian calculation in spiral galaxies are the result of the influence of neighbor galaxies, and that the v^2 of a particle in orbit of a spiral galaxy is the sum of the effects of F_s and the gravitational force F_g. Therefore,

$$v^2 = \frac{GM}{R} - G_\mathrm{s}\frac{m_\mathrm{s}}{m_\iota}\frac{L}{R} - \vec{R} \bullet \vec{a}_\mathrm{o} + |\vec{R} \times \vec{a}_\mathrm{o}| \,, \qquad (3)$$

where (1) the Newtonian simplifications of circular motion ($\ddot{R} = 0$) (Binney & Merrifield, 1998, p. 725) and a spherical mass density field are assumed, (2) the mass of the test particle is assumed to be constant over time, (3) M ($\mathrm{M}_\odot$) is the mass inside the sphere of radius R from Newton's spherical property, (4) the inertial mass m_ι equals gravitational mass m_g of the test particle (Will, 1993), (5) the L term is due to the F_s of the host galaxy, which also derives from a spherically symmetric ρ field; (6) $L = K_\epsilon \epsilon = 10^{-0.4 M_\mathrm{B}}$ erg s^{-1} for Source galaxies or $L = K_\eta \eta = -2.7 \times 10^{-0.4 M_\mathrm{B}}$ erg s^{-1} for Sink galaxies (Hodge, 2006); (7) $||$ indicates absolute value; and (8) $\vec{a}_\mathrm{o}$ (km s^{-2}) is the acceleration caused by neighboring galaxies,

$$\vec{a}_\mathrm{o} = \frac{G_\mathrm{s} m_\mathrm{s}}{m_\iota}\vec{\nabla}\rho \,, \qquad (4)$$

where the number of galaxies exclude the host galaxy. Note that no assumption about the significance of $\vec{a}_\mathrm{o}$ has been made.

Because v is measured only along the major axis in the region under consideration (Binney & Merrifield, 1998, p. 725) and if the $\vec{\nabla}\rho$ field is approximately uniform across a galaxy, Eq. (3) becomes

$$v^2 = G\frac{M}{R_\mathrm{major}} - \frac{G_\mathrm{s} m_\mathrm{s}}{m_\iota}\frac{L}{R_\mathrm{major}} + |\vec{K} \bullet \vec{a}_\mathrm{o}| R_\mathrm{major} \,, \qquad (5)$$

where $\vec{K}$ (km kpc^{-1}) is a constant vector and R_major (kpc) is the galactocentric radius along the major axis.

In Fig. 1 the H I RC at lower radius R_rr (kpc) in the RR has two scalloped shapes that suggests spherically symmetric shells of matter. Also, the Hα RC rapidly increases, peaks, and then declines at the beginning of each shell. The Hα lines are generally formed in excited interstellar gas. In the disk region of a galaxy, the gas is usually excited by hot stars (Binney & Merrifield, 1998). Because the m_s/m_ι factor must be different for different matter types, each shell has a different metallicity star type. Because the Hα RC approaches the H I RC in the disk region such as plotted in Fig. 1 with hot, hydrogen burning stars, the m_s/m_ι factor must be the same for H I and hydrogen stars. This suggests the m_s/m_ι factor varies by element type and acts on atoms at the largest. The metallicity - radius relation follows.

The m_s/m_ι ratio of stars is changing through changing elemental composition by nucleosynthesis in addition to accretion and emission of matter. Therefore, the H I RC is preferred to trace the forces influencing a galaxy outside the bulge. Because only the H I RC is considered in the calculations herein, the units used were $G_\mathrm{s} m_\mathrm{s}/m_\iota = 1$ kpc km^2 s^{-1} erg^{-1}.

Table 1: Data for the select galaxies.

Galaxy	morphology[a]	t[b]	lc[c]	RC[d]	D_{a}[e]
NGC 0224	SA(s)b	3	2	F	0.79
NGC 0300	SA(s)d	6.9	6	R	2.00
NGC 0598	SA(s)cd	6	4	R	0.84
NGC 0925	SAB(s)d HII	7	4	D	9.16
NGC 2403	SAB(s)cd	6	5	F	3.22
NGC 2841	SA(r)b;LINER Sy	3	1	F	14.07[f]
NGC 3031	SA(s)ab;LINER Sy1.8	2.4	2	D	3.63
NGC 3198	SB(rs)c	5.2	3	F	13.80
NGC 3319	SB(rs)cd;HII	5.9	3.3	R	13.30
NGC 4258	SAB(s)bc;LINER Sy1.9	4	3.9	D	7.98
NGC 4321	SAB(s)bc;LINER HII	4	1	D	15.21
NGC 4414	SA(rs)c? LINER	5.1	3.6	D	17.70
NGC 4535	SAB(s)c	5	1.9	D	15.78
NGC 4548	SBb(rs);LINER Sy	3.1	2	D	16.22
NGC 5457	SAB(rs)cd	5.9	1	D	6.70
NGC 7331	SA(s)b;LINER	3.9	2	F	14.72

---

[a] Galaxy morphological from the NED database.

[b] Galaxy morphological type code from the LEDA database.

[c] Galaxy luminosity class code from the LEDA database.

[d] Galaxy's H I RC type according to slope in the OR. R is rising, F is flat, and D is declining.

[e] The distance D_{a} (Mpc) to the galaxy from Freedman et al. (2001) unless otherwise noted.

[f] The D_{a} is from Macri et al. (2001).

3 Results

3.1 Sample

The elliptical, lenticular, irregular, and spiral galaxies used in the calculations were the same as used in Hodge (2006). That is, they were selected from the NED database[3]. The selection criteria were that the heliocentric redshift z_{mh} be less than 0.03 and that the object be classified as a galaxy. The parameters obtained from the NED database included the name, equatorial longitude E_{lon} (degrees) for J2000.0, equatorial latitude E_{lat} (degrees) for J2000.0, morphology, the B-band apparent magnitude m_{b} (mag.), and the extinction E_{xt} (mag.) as defined by NED. The galactocentric redshift z was calculated from z_{mh}.

The 21-cm line width W_{20} (km s^{-1}) at 20 percent of the peak, the inclination i_{n} (arcdegrees), the morphological type code "t", the luminosity class code "lc", and the position angle P_{a} (arcdegrees) for galaxies were obtained from the LEDA database[4] when such data existed.

The selection criteria for the "select galaxies" were that a H I RC was available in the literature and that D_{a} was available from Freedman et al. (2001) or Macri et al. (2001). Data for the 16 select galaxies are shown in Table 1 and their H I RCs are plotted in Fig. 2. The L for the select galaxies was calculated using D_{a}, m_{b}, and E_{xt}. The selection criteria for the other sample galaxies were that a H I RC was available in the literature and that the L could be calculated using the TF method with the constants developed in Hodge (2006).

This select galaxy sample has LSB, medium surface brightness (MSB), and high surface brightness (HSB) galaxies; has LINER, Sy, HII, and less active galaxies; has galaxies that have excellent and poor agreement between the distance D_{tf} (Mpc) calculated using the TF relation and D_{a}; has a D_{a} range of from 0.79 Mpc to 17.70 Mpc; has field and cluster galaxies; and has galaxies with rising, flat, and declining RCs.

---

[3] The Ned database is available at http://nedwww.ipac.caltech.edu. The data were obtained from NED on 5 May 2004.

[4] The LEDA database is available at http://leda.univ-lyon.fr. The data were obtained from LEDA on 5 May 2004.

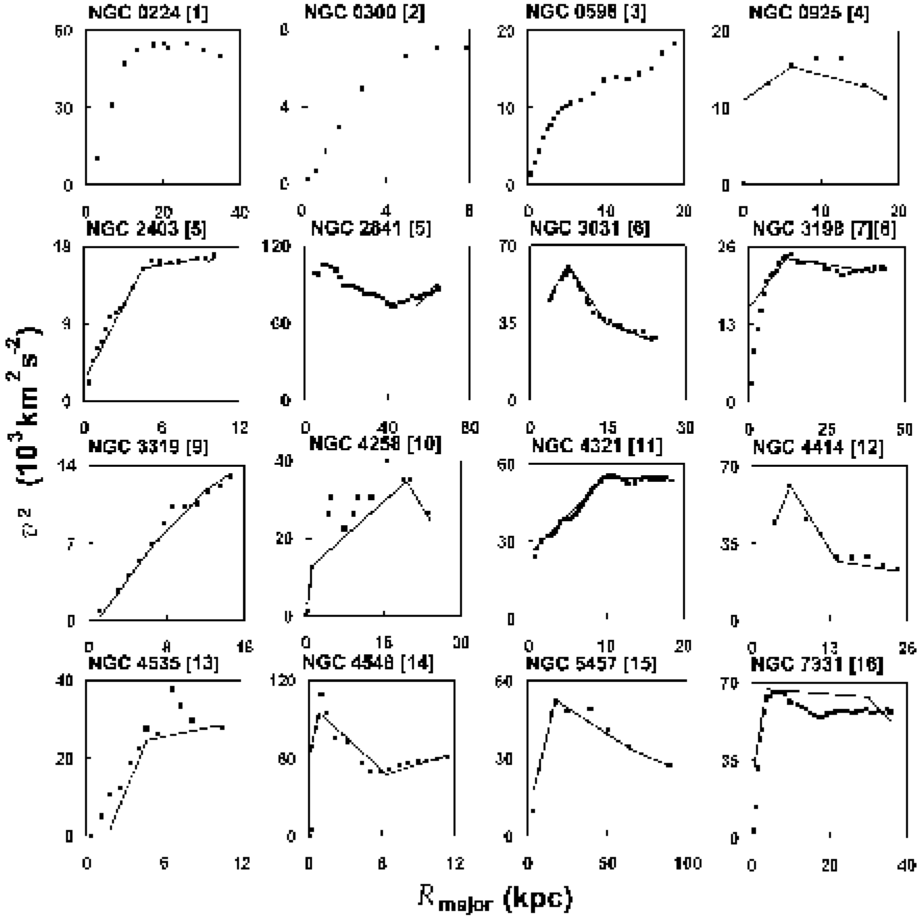

Figure 2: Plots of the square of the H I rotation velocity v^2 (10^3 km^2 s^{-2}) versus galactocentric radius R_{major} (kpc) along the major axis. The straight lines mark the application of the derived equations to the RCs of the select galaxies. The application of the derived equations to NGC 0224, NGC 0300, and NGC 0598 were omitted because these galaxies lacked a $|\vec{K} \bullet \vec{a}_{\mathrm{o}}|$ value. The references for the RCs are noted in brackets and are as follows: [1]Gottesman et al. (1966), [2]Carignan & Freeman (1985), [3]Corbelli & Salucci (2000), [4]Krumm & Salpeter (1979), [5]Begeman et al. (1991), [6]Rots (1975), [7]van Albada et al. (1985), [8]Bosma (1981), [9]Moore & Gottesman (1998), [10]van Albada & Shane (1975), [11]Sempere et al. (1995), [12]Braine et al. (1993), [13]Chincarini & de Souza (1985), [14]Vollmer et al. (1999), [15]Huchtmeier (1975), and [16]Mannheim & Kmetko (1996).

3.2 First approximation

When modeling an RC, the knee or turnover of an H I RC is often drawn smooth and relatively rounded. As depicted in Fig. 2 most of RCs of the selected galaxies have an abrupt change of slope at the turnover.

The end of the RR was found by fitting a least squares straight line to the first three data points, if available, inward and immediately before the knee of the RC with a 0.99 or higher correlation coefficient. NGC 2841 lacked data points to identify the RR. NGC 4414 had only two data points before the knee and a significant decline in v^2 to indicate the RR. The linear relation suggests a cylindrical distribution of matter in the RR near the knee.

At R_Δ, $v_\Delta \approx 0$ that implies the effective mass ≈ 0 inside a sphere with a R_Δ radius. That is, from Eq. (5) $M_\Delta \approx G_\mathrm{s} m_\mathrm{s} L / G m_\iota$, where M_Δ is the mass within R_Δ at which $\mathrm{d}v^2/\mathrm{d}R = 0$ and at which the RR begins.

The mass in an elemental volume $\mathrm{d}R$ in the RR near the turnover was modeled as a cylinder shell of small height H_rr (Binney & Merrifield, 1998, p. 724) and with density D_rr at R_rr. The mass M_rr within a sphere with a R_rr radius is

$$M_\mathrm{rr} = (D_\mathrm{rr} H_\mathrm{rr} 2\pi)\, R^2_\mathrm{rr} + M_\Delta + M_\mathrm{c}\,, \tag{6}$$

where M_c is a small correction term, the mass in the thin cylindrical RR shell $\approx$ the mass in the spherical shell with the same radial parameters, and the M_Δ is distributed in a much thicker volume, which may be spherical. The components of M_c are $-(D_\mathrm{rr} H_\mathrm{rr} 2\pi)\, R^2_\Delta$, the small amount of matter indicated by $v_\Delta \neq 0$, and the variation of the mass in the RR from a cylindrical distribution.

Inserting Eq. (6) into Eq. (5) for the RR yields

$$\begin{aligned} v^2_\mathrm{rr} \;=\;& \left(\frac{m_\mathrm{g}}{m_\iota} G D_\mathrm{rr} H_\mathrm{rr} 2\pi\right) R_\mathrm{rr} \\ &+ \frac{G(M_\Delta + M_\mathrm{c}) - m_\mathrm{s} G_\mathrm{s} L / m_\iota}{R_\mathrm{rr}} \\ &- |\vec{K} \bullet \vec{a}_\mathrm{o}| R_\mathrm{rr}\,, \end{aligned} \tag{7}$$

where v_rr (km s^{-1}) is the rotation velocity of H I in the RR at R_rr.

By averaging from side-to-side of the galaxy, the effect of the $|\vec{K} \bullet \vec{a}_\mathrm{o}|$ term was reduced and was considered insignificant for the first approximation compared to the D_rr term near the knee. The $\vec{F}_\mathrm{g}$ and the $\vec{F}_\mathrm{s}$ offset each other at R_Δ to produce a minimum v that then rises in the RR. Because $v_\Delta \approx 0$ and the RCs near the knee are well fit by the straight lines, the $[G(M_{\Delta\mathrm{r}} + M_\mathrm{c}) - m_\mathrm{s} G_\mathrm{s} L m_\iota^{-1}]/R_\mathrm{rr}$ term is small and nearly constant in the RR compared to the D_rr term near the knee of the RC. Equation (7) suggest v^2_rr depends on galaxy parameters D_rr and H_rr. Therefore, the first approximation is

$$\frac{v^2_\mathrm{rr}}{10^3\,\mathrm{km}^2\,\mathrm{s}^{-2}} = S_\mathrm{rr} \frac{R_\mathrm{rr}}{\mathrm{kpc}} + I_\mathrm{rr}\,, \tag{8}$$

where S_rr and I_rr are the slope and intercept of the linear $v^2_\mathrm{rr} - R_\mathrm{rr}$ relationship, respectively.

As R_rr increases, m_s/m_ι of the predominant mass increases and the predominant particles have decreasing density. Decreasing the amount of mass in a given cylindrical shell causes the end of the RR and the beginning of the transition region (TR) between the RR and OR. Because $\epsilon \propto M_{\mathrm{t}\epsilon}$ and $\epsilon \propto M_\Delta$, the mass M_rrmax within the maximum RR radius R_rrmax (kps) $\propto \epsilon \propto L$ of Eq. (5). The rotation velocity v_rrmax (km s^{-1}) of the galaxy at R_rrmax can be used to compare parameters among galaxies. Because this change is caused by the change in elemental types that depends on the ϵ and, hence, L of a galaxy, the end of the RR is occurring under similar conditions in all galaxies. Thus, the $v^2_{\rm rrmax}$ and $R_{\rm rrmax}$ are comparable parameters among galaxies. Posit, as a first approximation,

$$\frac{v^2_{\rm rrmax}}{10^3 {\rm km}^2\,{\rm s}^{-2}} = S_{\rm a}\frac{L}{10^8\,{\rm erg\,s}^{-1}} + I_{\rm a}\,, \tag{9}$$

where $S_{\rm a}$ and $I_{\rm a}$ are the slope and intercept of the linear relation, respectively.

When the error in calculating distance is a small factor such as when using $D_{\rm a}$ or $D_{\rm tf}$, more galaxies were sampled. The data of $v^2_{\rm rrmax}$ versus L of 15 select galaxies from Fig. 2 and of 80 other galaxies from Begeman et al. (1991); Broeils (1992); García-Ruiz et al. (2002); Guhathakurta et al. (1988); Kornreich et al. (2000, 2001); Liszt & Dickey (1995); Mannheim & Kmetko (1996); Rubin et al. (1985); and Swaters et al. (1999), for which the RR was identified, are plotted in Fig. 3. The other sample galaxies are listed in Table 2 denoted by an integer in the a_1 column. Some of the galaxies had only two data points and a significant decline in v^2 to indicate the end of the RR. The distribution of the data points in Fig. 3 suggested a grouping of the galaxies such that the $v^2_{\rm rrmax}$ versus L relations are linear for each group. This is reflected in the plotted lines in Fig. 3. Call each group a “classification”. For the calculation, the $(L, v^2_{\rm rrmax}) = (0,0)$ point was included in all classifications. The relationship of the slopes of the lines is

$$\log_{10} S_{\rm a} = S_{\rm ervd} a_1 + I_{\rm ervd}\,, \tag{10}$$

where a_1 is an integer, $S_{\rm ervd} = 1.3 \pm 0.2$ and $I_{\rm ervd} = 0.31 \pm 0.01$ were obtained by a least squares fit to produce the lowest uncertainty $\sigma_{\rm e}$. The $\sigma_{\rm e}$ was calculated as the standard deviation of the relative difference $(\delta v^2_{\rm rrmax}/v^2_{\rm rrmax})$ between the measured parameter value and the calculated parameter value divided by the calculated parameter value for the sample galaxies. Because the goal is to examine the slope of the lines and because the $(L, v^2_{\rm rrmax}) = (0,0)$ point was included in all lines, minimization of $\sigma_{\rm e}$ chooses the calculated line with the closest slope to the slope of the line from (0,0) to the data point. A χ^2 type of minimization would choose a different line for some of the sample galaxies.

Therefore,

$$S_{\rm a} = K_{\rm a_1} B^{a_1}_{\rm a_1}\,, \tag{11}$$

where $I_{\rm a} = 0$ and $K_{\rm a_1} = 1.3 \pm 0.2$ and $B_{\rm a_1} = 2.06 \pm 0.07$ at 1 σ. The values of $K_{\rm a_1}$ and $B_{\rm a_1}$ were chosen as the maximum $B_{\rm a_1}$ value that yielded a correlation coefficient for each of the lines from the origin to the data points (see Table 3 and Fig. 3) greater than 0.90, that yielded a minimum $\sigma_{\rm e}$, and that rejected the null hypothesis of the test in Appendix A with a confidence greater than 0.95.

Combining Eqs. (9) and (11) yields

$$\frac{v^2_{\rm rrmax}}{10^3\,{\rm km}^2\,{\rm s}^{-2}} = K_{\rm a_1} B^{a_1}_{\rm a_1}\frac{L}{10^8\,{\rm erg\,s}^{-1}} \pm \sigma_{\rm e}\,, \tag{12}$$

where $\sigma_{\rm e} = 21\%$. Note $\sigma_{\rm e} = 16\%$ for only the select galaxies. The large, filled circle in Fig. 3 denotes the data point for NGC 5448 $(\delta v^2_{\rm rrmax}/v^2_{\rm rrmax} = -0.35)$. The large, filled square in Fig. 3 denotes the data point for NGC 3031 $(\delta v^2_{\rm rrmax}/v^2_{\rm rrmax} = 0.25)$.

Tables 2 and 4 lists the a_1 values for the sample galaxies. Table 5 lists the minimum correlation coefficient $C_{\rm cmin}$ of the lines, the constants $K_{\rm x}$, and the exponential bases $B_{\rm x}$, where the subscript “x” denotes the generic term.

The average difference between L and the luminosity calculated using $D_{\rm tf}$ is $0.38L$ for the select galaxies. The relative difference in $v^2_{\rm rrmax}$ included the measurement uncertainty and the uncertainty that the RR may extend farther than the measured point such as seen for NGC 4258. The relative differences $\delta L/L = 0.3$ and $\delta v^2_{\rm rrmax}/v^2_{\rm rrmax} = 0.1$ are shown as error bars in Fig. 3 for the select galaxies.

Table 2: Interger values for the non-select galaxies in the sample.

Galaxy	a_1	a_2	f_1	f_2	j_1	j_2	Galaxy	a_1	a_2	f_1	f_2	j_1	j_2
IC 0467	3	9					NGC 4206	2	7				
IC 2233	4	6	4	0	1	5	NGC 4216	2	8				
NGC 0701	3	8					NGC 4222	5	10				
NGC 0753	4	8					NGC 4237	4	6				
NGC 0801	5	8					NGC 4359	4	3	3	1	1	5
NGC 0991	2	3	2	-3	1	3	NGC 4378	3	11				
NGC 1024	4	8					NGC 4388	5	5				
NGC 1035	4	6					NGC 4395	6	3	6	-1	-1	5
NGC 1042	3	4	3	-2	3	3	NGC 4448	4	7				
NGC 1085	5	6					NGC 4605	4	10				
NGC 1087	4	8					NGC 4647	3	7				
NGC 1169					4	5	NGC 4654	4	1				
NGC 1325	2	9					NGC 4682	3	7				
NGC 1353	5	6					NGC 4689	5	9				
NGC 1357	4	9					NGC 4698	4	6				
NGC 1417	5	9					NGC 4772					1	3
NGC 1421	3	4					NGC 4845	3	7				
NGC 1515	5	4					NGC 4866	4	9	4	7	3	4
NGC 1560	4	10	5	2			NGC 5023	4	8	4	-1	1	4
NGC 1620	3	5					NGC 5107					0	4
NGC 2715	2	7					NGC 5229	4	6	3	4	2	4
NGC 2742	3	5					NGC 5297	4	6	0	0	2	4
NGC 2770					3	4	NGC 5301	4	8	3	5	3	3
NGC 2844	3	13					NGC 5377					2	3
NGC 2903	5	11	3	5			NGC 5448	5	7	3	3	1	2
NGC 2998	3	2					NGC 5474	1	12	1	-2	0	4
NGC 3054	4	11					NGC 6503	5	9	5	4		
NGC 3067	5	15					NGC 6814	7	6	8	-3		
NGC 3109	5	5	5	2			NGC 7171	3	6				
NGC 3118	4	4	4	1	2	3	NGC 7217	4	8				
NGC 3200	4	15					NGC 7537	4	-1				
NGC 3432	4	10	4	6	4	5	NGC 7541	4	0				
NGC 3495	2	5					UGC 01281	4	5	4	-4	0	3
NGC 3593	5	11					UGC 02259	5	8	5	1		
NGC 3600	4	5	4	6	4	5	UGC 03137	5	9	3	4	3	5
NGC 3626					4	6	UGC 03685	4	7	5	-4	0	6
NGC 3672	3	8					UGC 05459	5	6	4	2	2	6
NGC 3900					1	3	UGC 07089	4	0	4	-2	0	4
NGC 4010	3	8	4	3	2	5	UGC 07125	4	4	4	-1	1	3
NGC 4051	3	7	1	3			UGC 07321	2	7	4	8	6	4
NGC 4062	4	5					UGC 07774	4	8	4	1	2	5
NGC 4096	4	7	3	-2	2	4	UGC 08246	3	2	3	-2	0	5
NGC 4138					2	5	UGC 09242					0	23
NGC 4144	3	6	4	1	2	6	UGC 10205	1	10				
NGC 4178	4	6											

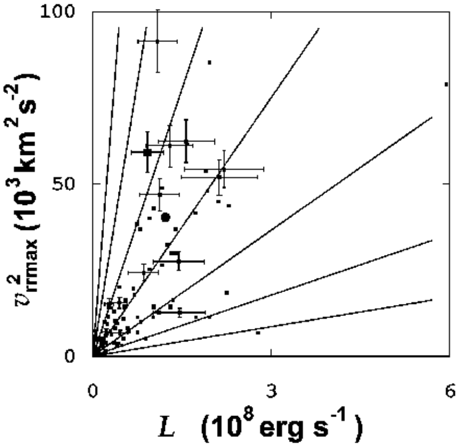

Figure 3: Plots of square of the rotation velocity $v^2_{\rm rrmax}$ (10^3km^2 s^{-2}) at the maximum extent of the RR versus B band luminosity L (10^8 erg s^{-1}) for the 95 sample galaxies. The 15 select galaxies have error bars that show the uncertainty range in each section of the plot. The error bars for the remaining galaxies are omitted for clarity. The straight lines mark the lines whose characteristics are listed in Table 3. The large, filled circle denotes the data point for NGC 5448. The large, filled square denotes the data point for NGC 3031.

Table 3: Data for the integer values of a_1 of Eq. (12) shown as the plotted lines in Fig. 3.

a_1[a]	No.[b]	Corr.[c]	F Test	$S_{\rm a}$[de]	$I_{\rm a}$[f]
1	2	1.00	1.00	2.482±0.004	0.006±0.006
2	7	0.97	0.93	6.6 ±0.6	0.1 ±0.7
3	20	0.99	0.96	12.8 ±0.5	-0.8 ±0.8
4	39	0.98	0.92	23.2 ±0.7	0.7 ±0.7
5	24	0.97	0.90	42 ±2	1 ±2
6	2	1.00	1.00	84.3 ±0.3	-0.2 ±0.2
7	1	1.00	1.00	261	0

---

[a] The integer denoting the exponential value in Eq. (12).

[b] The number of data points for each a_1 value.

[c] The correlation coefficient rounded to two decimal places.

[d] The least squares fit slope of the $v^2_{\rm rrmax}$ - L lines.

[e] The lines were calculated using (L,$v^2_{\rm rrmax}$) = (0,0) as a data point.

[f] The least squares fit intercept of the $v^2_{\rm rrmax}$ - L lines.

Table 4: First approximation integer values for the select galaxies.

Galaxy	a_1	b_1	c_1	d_1	e_1	f_1	g_1	h_1	i_1	j_1	k_1	l_1
NGC 0224	5	5	5	3	4	4	3	3	4			4
NGC 0598	4	6	3	6	6	5	5	3	6			6
NGC 3031	5	5	5	5	4	3	3	2	4	3	5	7
NGC 0300	5	7	3	6	7	5	5	2	7			7
NGC 2403	5	6	4	6	6	4	4	2	6	1	4	6
NGC 5457	4	5	5	1	2	1	4	3	1	4	5	4
NGC 4258	3	2	1	4	5	2	2	2	3	2	1	2
NGC 0925	5	6	4	4	2	2	4	2	4	2	3	6
NGC 2841		1				4	4	4	3	2	5	1
NGC 3198	4	6	5	2	1	2	4	3	3	2	6	5
NGC 4414	5	4	4	4	4	2	3	2	3	1	2	6
NGC 3319	3	6	4	2	3	3	4	2	5	1	5	4
NGC 7331	5	3	3	5	5	3	3	3	4	3	3	4
NGC 4535	4	4	3	3	4	2	1	1	5	3	4	3
NGC 4321	4	4	4	2	2	2	1	2	4	3	2	3
NGC 4548	6	1	2	10	8	4	2	2	6	9	16	7

Other parametric relationships to L in the RR were calculated using the same procedure that was used to evaluate the v^2_{rrmax} - L relation. Because these equations involved R_{rrmax}, the calculation considered only the 15 select galaxies. The resulting equations are:

$$\frac{R_{\mathrm{rrmax}}}{\mathrm{kpc}} = K_{\mathrm{b}_1}\, B_{\mathrm{b}_1}^{b_1}\, \frac{L}{10^8\,\mathrm{erg\,s^{-1}}} \pm 14\%\,; \tag{13}$$

$$\frac{R_{\mathrm{rrmax}} v^2_{\mathrm{rrmax}}}{10^3\,\mathrm{kpc\,km^2\,s^{-2}}} = K_{\mathrm{c}_1}\, B_{\mathrm{c}_1}^{c_1}\, \frac{L}{10^8\,\mathrm{erg\,s^{-1}}} \pm 15\%\,; \tag{14}$$

$$\frac{v^2_{\mathrm{rrmax}}/R_{\mathrm{rrmax}}}{10^3\,\mathrm{kpc^{-1}\,km^2\,s^{-2}}} = K_{\mathrm{d}_1}\, B_{\mathrm{d}_1}^{d_1}\, \frac{L}{10^8\,\mathrm{erg\,s^{-1}}} \pm 11\%\,;\ \text{and} \tag{15}$$

$$\frac{S_{\mathrm{rr}}}{10^3\,\mathrm{kpc^{-1}\,km^2\,s^{-2}}} = K_{\mathrm{e}_1}\, B_{\mathrm{e}_1}^{e_1}\, \frac{L}{10^8\,\mathrm{erg\,s^{-1}}} \pm 13\%\,; \tag{16}$$

where first approximation integer values are listed in Table 4 and the C_{cmin}, K_{x}, and B_{x} are listed in Table 5.

Equations (12)–(15) suggest at least two of the four integers a_1, b_1, c_1, and d_1 are functions of the other two.

The end of the EOR was considered to be at the largest radius R_{eormax} (kpc) along the major axis that H I is in orbit around the galaxy. Several galaxies have a H I measured point on one side of the galaxy at a greater R_{major} than the other side. Because averaging the v from each side of the galaxy was required to reduce the $|\vec{K} \bullet \vec{a}_{\mathrm{o}}|$ effect that causes non-circular rotation, the outermost measured point used in the calculations was at the R_{eormax} with data points on both sides of the galaxy. At $R > R_{\mathrm{eormax}}$ particles are no longer in orbit. For particles other than H I, the m_{s}/m_{ι} is less. Therefore, their maximum radius in a galaxy is less. NGC 4321 has H I extending farther than a radius of four arcminutes. However, Knapen et al. (1993) concluded the H I motion beyond four arcminutes is not disk rotation. Therefore, R_{eormax} was considered to be at four arcminutes for NGC 4321.

Because $\epsilon \propto M_{\mathrm{t}\epsilon}$ and $\epsilon \propto M_{\Delta}$, $M_{\mathrm{eormax}} \propto \epsilon \propto L$, where M_{eormax} is the mass within R_{eormax} of Eq. (5). The rotation velocity v_{eormax} of the galaxy at a radius of R_{eormax} can be used to compare parameters among galaxies.

Table 5: Values of the minimum correlation coefficients C_{cmin}, constants K_{x}, and exponent bases B_{x} for the first approximation equations.

Integer[a]	C_{cmin}[b]	K_{x}[c]	B_{x}[d]
a_1	0.97	1.3 ± 0.2	2.06±0.07
b_1	0.86	0.34 ± 0.04	1.88±0.05
c_1	0.96	19 ± 1	1.89±0.05
d_1	0.99	1.0 ± 0.1	1.57±0.06
e_1	0.97	0.49 ± 0.06	1.71±0.04
f_1	0.96	8.6 ± 0.7	1.57±0.04
g_1	0.93	4.4 ± 0.4	1.77±0.06
h_1	0.97	150 ±10	2.5 ±0.1
i_1	0.95	0.09 ± 0.02	1.9 ±0.2
l_1	0.96	0.075± 0.009	1.95±0.02

---

[a] The integer of the exponential value of parametric relationship that denotes the applicable equation.

[b] The minimum correlation coefficient rounded to two decimal places of the lines of the parametric relationship.

[c] The constant of proportionality at 1σ of the parametric relationship.

[d] The exponent base at 1σ of the parametric relationship.

Parameter relations to L in the EOR were calculated using the same procedure used to evaluate the $v^2_{\mathrm{rrmax}} - L$ relation.

The data of v^2_{eormax} versus L of 16 select galaxies and of 34 other galaxies from Begeman et al. (1991); Broeils (1992); García-Ruiz et al. (2002); Kornreich et al. (2000, 2001); Liszt & Dickey (1995); Mannheim & Kmetko (1996); and Swaters et al. (1999) for a total of 50 sample galaxies are plotted in Fig. 4. The 34 other galaxies are listed in Table 2 denoted by an integer in the f_1 column. The uncertainty in determining the value of the outermost point of the EOR is greater than determining the end of the RR. Because the determination of the outermost value of the parameters requires instrumentation sensitive enough to measure the values, data prior to 1990 of 46 other galaxies used in the $v^2_{\mathrm{rrmax}} - L$ relation were omitted. The equations involving R_{eormax} used only the 16 select galaxies.

The resulting equations are:

$$\frac{v^2_{\mathrm{eormax}}}{10^3\,\mathrm{km}^2\,\mathrm{s}^{-2}} = K_{\mathrm{f}_1}\, B^{f_1}_{\mathrm{f}_1}\, \frac{L}{10^8\,\mathrm{erg}\,\mathrm{s}^{-1}} \pm 13\%\,, \tag{17}$$

where the large, filled circle in Fig. 4 denotes the data point for NGC 5448 ($\delta v^2_{\mathrm{eormax}}/v^2_{\mathrm{eormax}} = -0.20$) and the large, filled square denotes the data point for NGC 3031 ($\delta v^2_{\mathrm{eormax}}/v^2_{\mathrm{eormax}} = -0.08$);

$$\frac{R_{\mathrm{eormax}}}{\mathrm{kpc}} = K_{\mathrm{g}_1}\, B^{g_1}_{\mathrm{g}_1}\, \frac{L}{10^8\,\mathrm{erg}\,\mathrm{s}^{-1}} \pm 16\%\,; \tag{18}$$

$$\frac{R_{\mathrm{eormax}} v^2_{\mathrm{eormax}}}{10^3\,\mathrm{kpc}\,\mathrm{km}^2\,\mathrm{s}^{-2}} = K_{\mathrm{h}_1}\, B^{h_1}_{\mathrm{h}_1}\, \frac{L}{10^8\,\mathrm{erg}\,\mathrm{s}^{-1}} \pm 19\%\,;\ \text{and} \tag{19}$$

$$\frac{v^2_{\mathrm{eormax}}/R_{\mathrm{eormax}}}{10^3\,\mathrm{kpc}^{-1}\,\mathrm{km}^2\,\mathrm{s}^{-2}} = K_{\mathrm{i}_1}\, B^{i_1}_{\mathrm{i}_1}\, \frac{L}{10^8\,\mathrm{erg}\,\mathrm{s}^{-1}} \pm 15\%\,; \tag{20}$$

where first approximation integer values are listed in Tables 2 and 4 and the C_{cmin}, K_{x}, and B_{x} are listed in Table 5.

The uncertainty in calculating $|\vec{K} \bullet \vec{a}_{\mathrm{o}}|$ depends on the accuracy of measuring the distance D (Mpc) to neighbor galaxies that are without a D_{a} and without a D_{tf} measurement. The cell structure of galaxy clusters (Aaronson et al., 1982; Ceccarelli et al., 2005; Hodge, 2006; Hudson et al., 2004; Lilje et al., 1986; Rejkuba, 2004) suggests a systematic error in z relative to D of a galaxy. Therefore, using z and the Hubble Law to determine D introduces a large error.

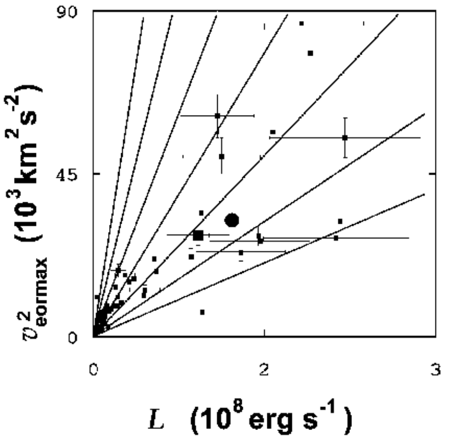

Figure 4: Plots of the square of the H I rotation velocity $v^2_{\rm eormax}$ ($10^3\,{\rm km}^2\,{\rm s}^{-2}$) at extreme outer region versus B band luminosity L ($10^8\,{\rm erg\,s}^{-1}$) for the 50 sample galaxies. The 16 select galaxies have error bars that show the uncertainty level in each section of the plot. The error bars for the remaining galaxies are omitted for clarity. The large, filled circle denotes the data point for NGC 5448. The large, filled square denotes the data point for NGC 3031.

However, the cell model also suggests neighboring galaxies have a similar D/z ratio in the first approximation. For those few galaxies near our line of sight to the sample galaxy and near the sample galaxy, Hodge (2006) found a z change caused by the light passing close to galaxies. For a single galaxy this effect is small and was ignored. Therefore,

$$D_i = \frac{z_i}{z_p} D_p \,, \tag{21}$$

where z_p and D_p (Mpc) are the redshift and distance of the sample galaxy, respectively, and z_i and D_i (Mpc) are the redshift and calculated distance of the i^{th} neighbor galaxy, respectively. The $D_p = D_{\rm a}$ for the select galaxies and $D_p = D_{\rm tf}$ for the other sample galaxies. The L of the i^{th} neighbor galaxy was calculated using D_i, $m_{\rm b}$, and $E_{\rm xt}$.

Because larger $|z_i - z_p|$ implies larger error in D_i, the $N_{\rm sources}$ and $N_{\rm sinks}$ of Eq. (4) was limited to the number N of galaxies with the largest influence on $|\vec{\nabla}\rho|$ of the sample galaxy, where the $\vec{\nabla}\rho$ of Eq. (4) is evaluated at the center of the sample galaxy. The $N = 7$ was chosen because it produced the highest correlation in the calculations. Also, $6 \leq N \leq 9$ produced acceptable correlation in the calculations.

The calculation of $|\vec{K} \bullet \vec{a}_{\rm o}|$ also requires knowledge of the orientation of the sample galaxy. The direction of the sample galaxy's polar unit vector $\vec{e}_{\rm polar}$ was defined as northward from the center of the sample galaxy along the polar axis of the galaxy. Hu et al. (2006); Pereira & Kuhn (2005); and Trujillo et al. (2006) found an alignment of the polar axis of neighboring spiral galaxies. Therefore, the orientation of $\vec{e}_{\rm polar}$ with the higher $|\vec{e}_{\rm polar} \bullet \vec{a}_{\rm o}|$ was chosen for the calculations.

The major axis unit vector $\vec{e}_{\rm major}$ was defined as eastward from the center of the sample galaxy along the major axis of the galaxy. The minor axis unit vector $\vec{e}_{\rm minor} \equiv \vec{e}_{\rm major} \times \vec{e}_{\rm polar}$.

At equal $R_{\rm major} > R_{\rm rrmax}$ on opposite sides of the galaxy, the L terms of Eq. (5) are equal and the M terms are nearly equal. Define asymmetry $A_{\rm sym}$,

$$A_{\rm sym} \equiv (v^2_{\rm h} - v^2_{\rm l})|_R \,, \tag{22}$$

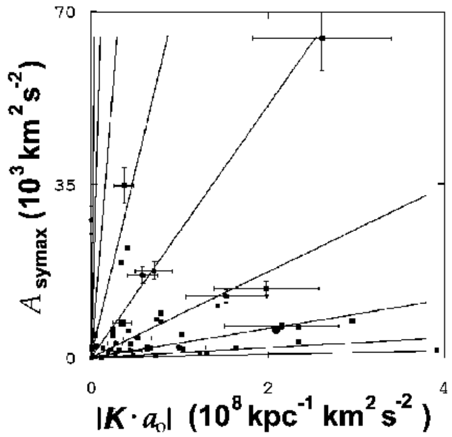

Figure 5: Plots of maximum asymmetry A_{symax} ($10^3\,\text{km}^2\,\text{s}^{-2}$) versus $|\vec{K} \bullet \vec{a}_{\text{o}}|$ ($10^3\,\text{kpc}^{-1}\,\text{km}^2\,\text{s}^{-2}$) for the 50 sample galaxies. The 13 select galaxies have error bars that show the uncertainty level in each section of the plot. . The error bars for the remaining galaxies are omitted for clarity. The large, filled circle denotes the data point for NGC 5448. The large, filled square denotes the data point for NGC 3031.

where v_{h} and v_{l} are the larger v and smaller v at the same R_{major} ($|_R$) on opposite sides of the galaxy, respectively.

The A_{sym} is a function of R_{major}. The A_{sym} and $|\vec{K} \bullet \vec{a}_{\text{o}}|$ are sensitive to both radial (non-circular) motion of particles and to variation of v due to torque. For the first approximation the maximum asymmetry A_{symax} in the OR depends predominately on $|\vec{K} \bullet \vec{a}_{\text{o}}|$. Because A_{symax} is minimally dependant on R, A_{symax} is comparable among galaxies.

NGC 0224, NGC 0300, and NGC 0598 were omitted from the sample because their $z < 0$ and their neighbor galaxies may have positive or negative z. Therefore, evaluating the distance of neighbor galaxies of these galaxies was considered unreliable. Table 6 lists the $|\vec{K} \bullet \vec{a}_{\text{o}}|$, A_{symax}, and A_{symax} references for the remaining 13 select galaxies. The sample consisted of 13 select galaxies and of 36 other galaxies from García-Ruiz et al. (2002); Kornreich et al. (2000, 2001); and Swaters et al. (1999) for a total of 49 sample galaxies. The 36 other galaxies are listed in Table 2 denoted by an integer in the j_1 column. The plot of A_{symax} versus $|\vec{K} \bullet \vec{a}_{\text{o}}|$ is shown in Fig. 5.

The same procedure that was used to evaluate the $v^2_{\text{rrmax}} - L$ relation was used to evaluate the $A_{\text{symax}} - |\vec{K} \bullet \vec{a}_{\text{o}}|$ relation. The result is

$$\frac{A_{\text{symax}}}{10^3\,\text{km}^2\,\text{s}^{-2}} = K_{\text{j}_1} B_{\text{j}_1}^{j_1} \frac{|\vec{K} \bullet \vec{a}_{\text{o}}|}{10^3\,\text{kpc}^{-1}\,\text{km}^2\,\text{s}^{-2}} \pm 28\%\,, \tag{23}$$

where first approximation integer values are listed in Tables 2 and 4, $C_{\text{cmin}} = 0.98$, $K_{\text{j}_1} = (1.000 \pm 0.001)$, $B_{\text{j}_1} = 2.94 \pm 0.09$, and

$$\begin{aligned} \vec{K} \;=\; & (3.60 \times 10^{-6})\,\vec{e}_{\text{polar}} \\ & -(6.81 \times 10^{-6})\,\vec{e}_{\text{major}} \\ & -(1.18 \times 10^{-5})\,\vec{e}_{\text{minor}}\,\text{km}\,\text{kpc}^{-1} \end{aligned} \tag{24}$$

at 1σ. The value of $\vec{K}$ was chosen such that $K_{\text{j}_1} \approx 1.00$.

The large, filled circle in Fig. 5 denotes the data point for NGC 5448 ($\delta A_{\text{symax}}/A_{\text{symax}} = -0.08$). The large, filled square denotes the data point for

Table 6: Asymmetry and $|\vec{K} \bullet \vec{a}_{\mathrm{o}}|$ data for the select galaxies.

Galaxy	A_{symax} [a]	$\lvert\vec{K} \bullet \vec{a}_{\mathrm{o}}\rvert$ [b]	Ref. [c]
NGC 0925	12.5	1.53	[1]
NGC 2403	2.0	0.99	[2]
NGC 2841	4.0	0.52	[3][4]
NGC 3031	7.1	0.35	[4]
NGC 3198	2.9	0.27	[5][6]
NGC 3319	1.4	0.44	[7]
NGC 4258	14.0	2.0	[8]
NGC 4321	64.7	2.6	[9]
NGC 4414	6.5	2.2	[10]
NGC 4535	16.7	0.58	[11]
NGC 4548	27.9	0.0018	[12]
NGC 5457	34.8	0.37	[13]
NGC 7331	17.6	0.71	[6]

---

[a] The units are 10^3 km^2 s^{-2}. The uncertainty is ±10%.

[b] The units are 10^3 kpc^{-1} km^2 s^{-2}. The uncertainty is ±30%.

[c] References: [1]Krumm & Salpeter (1979), [2]Begeman et al. (1991), [3] Fillmore et al. (1986), [4]Rots (1975), [5]van Albada et al. (1985), [6]Bosma (1981), [7]Moore & Gottesman (1998), [8]van Albada & Shane (1975), [9]Sempere et al. (1995), [10]Braine et al. (1993), [11]Chincarini & de Souza (1985), [12]Vollmer et al. (1999), and [13]Bosma et al. (1981).

NGC 3031 ($\delta A_{\mathrm{symax}}/A_{\mathrm{symax}} = -0.21$). For the 13 select galaxies, $\sigma_{\mathrm{e}} = 17\%$ [excluding the $(A_{\mathrm{symax}}, |\vec{K} \bullet \vec{a}_{\mathrm{o}}|) = (0,0)$ point].

Because the net effect of F_{s} and F_{g} from the host galaxy is weak at the outer edge of the galaxy, the slope S_{eor} (kpc^{-1} km^2 s^{-2}) of the H I RC for the end of the EOR was compared among the 13 select galaxies. The S_{eor} were found by fitting a least squares straight line to the outermost two or more data points of the RC with a 0.97 or higher correlation coefficient. The same procedure that was used to evaluate the $v^2_{\mathrm{rrmax}} - L$ relation was used to evaluate the $S_{\mathrm{eor}} - |\vec{K} \bullet \vec{a}_{\mathrm{o}}|$ relation. The result is

$$\begin{aligned}\frac{S_{\mathrm{eor}}}{10^3\mathrm{kpc}^{-1}\,\mathrm{km}^2\,\mathrm{s}^{-2}} &= K_{\mathrm{k}_1} B_{\mathrm{k}_1}^{k_1} \frac{|\vec{K} \bullet \vec{a}_{\mathrm{o}}|}{10^3\mathrm{kpc}^{-1}\,\mathrm{km}^2\,\mathrm{s}^{-2}} \\ &\quad + I_{\mathrm{seor}} \pm 15\%\,, \qquad (25)\end{aligned}$$

where $C_{\mathrm{cmin}} = 0.96$, $K_{\mathrm{k}_1} = 0.64 \pm 0.09$, $B_{\mathrm{k}_1} = 1.74 \pm 0.06$, and $I_{\mathrm{seor}} = -4.8 \pm 0.1$ at 1σ. Tables 4 lists the k_1 values for the 13 select galaxies.

As seen in Fig. 2 the measured points in the OR appear nearly linear rather than a smoothly varying curve in most of the select galaxies. Therefore, the linear approximation of the RC slope in the OR was considered more appropriate than a smoothly varying function. Define S_{or} (km^2 s^{-2} kpc^{-1}) as the slope from the R_{rrmax} data point to the beginning of the S_{eor} of the H I RC. For the 15 select galaxies excluding NGC 2841, following the same procedure as for finding Eq. (12) yields

$$\frac{S_{\mathrm{or}}}{10^3\,\mathrm{km}^2\,\mathrm{s}^{-2}\,\mathrm{kpc}^{-1}} = -\,K_{\mathrm{l}_1}\,B_{\mathrm{l}_1}^{l_1}\,\frac{L}{10^8\,\mathrm{erg\,s}^{-1}} + I_{\mathrm{or}} \pm 15\%\,, \qquad (26)$$

where the integer values are listed in Table 4. The C_{cmin}, K_{l_1}, and B_{l_1} values are listed in Table 5 and $I_{\mathrm{or}} = 1.6 \pm 0.1$.

3.3 Second approximation

Equation (5) indicates the parameters of galaxies depend on L and $|\vec{K}\bullet\vec{a}_{\rm o}|$. The first approximation selected either L or $|\vec{K}\bullet\vec{a}_{\rm o}|$ depending upon which is predominant. The second approximation considered the less predominant term to be a systematic correction term. Posit the residual between the measured parameter value and the calculated first approximation parameter value is proportional to the less predominant term. Appling the same procedure as for finding Eq. (12) yields:

$$\frac{v^2_{\rm rrmax}}{10^3\,{\rm km^2\,s^{-2}}} = K_{\rm a_1}\, B^{a_1}_{\rm a_1}\,\frac{L}{10^8\,{\rm erg\,s^{-1}}} + (-1)^{s_a} K_{\rm a_2} B^{a_2}_{\rm a_2}\frac{|\vec{K}\bullet\vec{a}_{\rm o}|}{10^3\,{\rm kpc^{-1}\,km^2\,s^{-2}}} \pm 10\%\,, \tag{27}$$

where $K_{a_2} = 0.15\pm0.02$, $B_{\rm a_2} = 2.00\pm0.03$ at 1σ, for NGC 5448 ($\delta v^2_{\rm rrmax}/v^2_{\rm rrmax} = -0.04$), and for NGC 3031 ($\delta v^2_{\rm rrmax}/v^2_{\rm rrmax} = -0.03$);

$$\frac{R_{\rm rrmax}}{\rm kpc} = K_{\rm b_1}\, B^{b_1}_{\rm b_1}\,\frac{L}{10^8\,{\rm erg\,s^{-1}}} + (-1)^{s_b} K_{\rm b_2} B^{b_2}_{\rm b_2}\frac{|\vec{K}\bullet\vec{a}_{\rm o}|}{10^3\,{\rm kpc^{-1}\,km^2\,s^{-2}}} \pm 2\%\,, \tag{28}$$

where $K_{\rm b_2} = 0.08 \pm 0.01$ and $B_{\rm b_2} = 1.75 \pm 0.08$ at 1σ;

$$\frac{R_{\rm rrmax} v^2_{\rm rrmax}}{10^3\,{\rm kpc\,km^2\,s^{-2}}} = K_{\rm c_1}\, B^{c_1}_{\rm c_1}\,\frac{L}{10^8\,{\rm erg\,s^{-1}}} + (-1)^{s_c} K_{\rm c_2} B^{c_2}_{\rm c_2}\frac{|\vec{K}\bullet\vec{a}_{\rm o}|}{10^3\,{\rm kpc^{-1}\,km^2\,s^{-2}}} \pm 3\%\,, \tag{29}$$

where $K_{\rm c_2} = 0.63 \pm 0.07$ and $B_{\rm c_2} = 1.98 \pm 0.03$ at 1σ;

$$\frac{v^2_{\rm rrmax}/R_{\rm rrmax}}{10^3\,{\rm kpc^{-1}\,km^2\,s^{-2}}} = K_{\rm d_1}\, B^{d_1}_{\rm d_1}\,\frac{L}{10^8\,{\rm erg\,s^{-1}}} + (-1)^{s_d} K_{\rm d_2} B^{d_2}_{\rm d_2}\frac{|\vec{K}\bullet\vec{a}_{\rm o}|}{10^3\,{\rm kpc^{-1}\,km^2\,s^{-2}}} \pm 3\%\,, \tag{30}$$

where $K_{\rm d_2} = 0.024 \pm 0.007$ and $B_{\rm d_2} = 2.2 \pm 0.3$ at 1σ;

$$\frac{S_{\rm rr}}{10^3\,{\rm kpc^{-1}\,km^2\,s^{-2}}} = K_{\rm e_1}\, B^{e_1}_{\rm e_1}\,\frac{L}{10^8\,{\rm erg\,s^{-1}}} + (-1)^{s_e} K_{\rm e_2} B^{e_2}_{\rm e_2}\frac{|\vec{K}\bullet\vec{a}_{\rm o}|}{10^3\,{\rm kpc^{-1}\,km^2\,s^{-2}}} \pm 2\%\,, \tag{31}$$

where $K_{\rm e_2} = 0.021 \pm 0.003$ and $B_{\rm e_2} = 1.72 \pm 0.03$ at 1σ;

$$\frac{v^2_{\rm eormax}}{10^3\,{\rm km^2\,s^{-2}}} = K_{\rm f_1}\, B^{f_1}_{\rm f_1}\,\frac{L}{10^8\,{\rm erg\,s^{-1}}} + (-1)^{s_f} K_{\rm f_2} B^{f_2}_{\rm f_2}\frac{|\vec{K}\bullet\vec{a}_{\rm o}|}{10^3\,{\rm kpc^{-1}\,km^2\,s^{-2}}} \pm 2\%\,, \tag{32}$$

where $K_{\rm f_2} = 0.7\pm0.1$ and $B_{\rm f_2} = 1.9\pm0.1$ at 1σ, for NGC 5448 ($\delta v^2_{\rm eormax}/v^2_{\rm eormax} = -0.03$), and for NGC 3031 ($\delta v^2_{\rm eormax}/v^2_{\rm eormax} = -0.02$);

$$\frac{R_{\rm eormax}}{\rm kpc} = K_{\rm g_1}\, B^{g_1}_{\rm g_1}\,\frac{L}{10^8\,{\rm erg\,s^{-1}}} + (-1)^{s_g} K_{\rm g_2} B^{g_2}_{\rm g_2}\frac{|\vec{K}\bullet\vec{a}_{\rm o}|}{10^3\,{\rm kpc^{-1}\,km^2\,s^{-2}}} \pm 3\%\,, \tag{33}$$

where $K_{\rm g_2} = 0.008 \pm 0.002$ and $B_{\rm g_2} = 2.05 \pm 0.09$ at 1σ;

$$\frac{R_{\rm eormax} v^2_{\rm eormax}}{10^3\,{\rm kpc\,km^2\,s^{-2}}} = K_{\rm h_1}\, B^{h_1}_{\rm h_1}\,\frac{L}{10^8\,{\rm erg\,s^{-1}}} + (-1)^{s_h} K_{\rm h_2} B^{h_2}_{\rm h_2}\frac{|\vec{K}\bullet\vec{a}_{\rm o}|}{10^3\,{\rm kpc^{-1}\,km^2\,s^{-2}}} \pm 3\%\,, \tag{34}$$

where $K_{\rm h_2} = 7 \pm 2$ and $B_{\rm h_2} = 2.06 \pm 0.08$ at 1σ;

$$\frac{v^2_{\rm eormax}/R_{\rm eormax}}{10^3\,{\rm kpc^{-1}\,km^2\,s^{-2}}} = K_{\rm i_1}\, B^{i_1}_{\rm i_1}\,\frac{L}{10^8\,{\rm erg\,s^{-1}}} + (-1)^{s_i} K_{\rm i_2} B^{i_2}_{\rm i_2}\frac{|\vec{K}\bullet\vec{a}_{\rm o}|}{10^3\,{\rm kpc^{-1}\,km^2\,s^{-2}}} \pm 2\%\,, \tag{35}$$

where $K_{\rm i_2} = 0.024 \pm 0.002$ and $B_{\rm i_2} = 1.78 \pm 0.04$ at 1σ;

$$\frac{A_{\rm symax}}{10^3\,{\rm km^2\,s^{-2}}} = K_{\rm j_1} B^{j_1}_{\rm j_1}\,\frac{|\vec{K}\bullet\vec{a}_{\rm o}|}{10^3\,{\rm kpc^{-1}\,km^2\,s^{-2}}} + (-1)^{s_j} K_{\rm j_2} B^{j_2}_{\rm j_2}\frac{L}{10^8\,{\rm erg\,s^{-1}}} \pm 8\%\,, \tag{36}$$

Table 7: Second approximation integer values for the select galaxies.

Galaxy	a_2	b_2	c_2	d_2	e_2	f_2	g_2	h_2	i_2	j_2	k_2	l_2
NGC 0224												
NGC 0598												
NGC 3031	8	1	7	6	4	4	3	6	1	4	3	11
NGC 0300												
NGC 2403	3	3	4	4	6	2	4	2	5	5	5	6
NGC 5457	4	6	7	5	8	3	7	7	4	5	3	8
NGC 4258	4	2	1	3	6	2	4	3	2	4	2	1
NGC 0925	5	2	2	2	1	1	3	1	1	4	6	3
NGC 2841						5	8	8	4	2	4	1
NGC 3198	6	6	9	1	2	5	8	6	4	3	2	7
NGC 4414	4	3	6	4	6	2	5	2	1	1	1	6
NGC 3319	4	4	6	2	4	3	7	3	5	2	6	7
NGC 7331	7	3	6	6	7	3	6	5	5	2	3	3
NGC 4535	7	6	5	4	9	3	4	2	7	4	3	6
NGC 4321	1	1	2	1	2	2	1	3	3	3	1	5
NGC 4548	16	12	8	16	21	13	14	13	16	4	5	18

where $K_{\mathrm{j}_2} = 0.053 \pm 0.008$ and $B_{\mathrm{j}_2} = 2.4 \pm 0.2$ at 1σ [for the select galaxies, $\sigma_{\mathrm{e}}(\delta A_{\mathrm{symax}}/A_{\mathrm{symax}}) = -0.04$], for NGC 5448 ($\delta A_{\mathrm{symax}}/A_{\mathrm{symax}} = -0.02$), and for NGC 3031 ($\delta A_{\mathrm{symax}}/A_{\mathrm{symax}} = -0.04$);

$$\frac{S_{\mathrm{eor}}}{10^3\,\mathrm{kpc}^{-1}\,\mathrm{km}^2\,\mathrm{s}^{-2}} = K_{\mathrm{k}_1} B_{\mathrm{k}_1}^{k_1} \frac{|\vec{K} \bullet \vec{a}_{\mathrm{o}}|}{10^3\,\mathrm{kpc}^{-1}\,\mathrm{km}^2\,\mathrm{s}^{-2}} + I_{\mathrm{seor}} + (-1)^{s_k} K_{\mathrm{k}_2} B_{\mathrm{k}_2}^{k_2} \frac{L}{10^8\,\mathrm{erg\,s}^{-1}} \pm 2\%\,, \quad (37)$$

where $K_{\mathrm{k}_2} = 0.061 \pm 0.006$ and $B_{\mathrm{k}_2} = 1.80 \pm 0.05$ at 1σ; and

$$\frac{S_{\mathrm{or}}}{10^3\,\mathrm{km}^2\,\mathrm{s}^{-2}\,\mathrm{kpc}^{-1}} = -K_{\mathrm{l}_1} B_{\mathrm{l}_1}^{l_1} \frac{L}{10^8\,\mathrm{erg\,s}^{-1}} + I_{\mathrm{or}} + (-1)^{s_l} K_{\mathrm{l}_2} B_{\mathrm{l}_2}^{l_2} \frac{|\vec{K} \bullet \vec{a}_{\mathrm{o}}|}{10^3\,\mathrm{kpc}^{-1}\,\mathrm{km}^2\,\mathrm{s}^{-2}} \pm 2\%\,, \quad (38)$$

where $K_{\mathrm{l}_2} = 0.0039 \pm 0.0005$ and $B_{\mathrm{l}_2} = 1.96 \pm 0.05$ at 1σ. If the measured value of a parameter is larger than the first approximation calculated value, the sign $s_x = 0$ in Eqs. (27)-(38). If the measured value of a parameter is smaller than the first approximation calculated value, the sign $s_x = 1$ in Eqs. (27)-(38). The second approximation integer values are listed in Tables 2 and 7.

The calculated RCs of the above equations are plotted as solid lines in Fig. 2 for the select galaxies.

Because barred galaxies were part of the sample, the monopole Source suggests the ρ is not sourced by matter as is gravity. The Source appears as a monopole at the beginning of the RR that is a few kpc from the center of the galaxy.

4 Discussion and conclusion

The SPM L first approximation correlation with RC parameters is an expansion of the URC concept. The SPM includes observations such as rapidly declining RCs and asymmetric RCs.

The second approximation equations show little effect of neighboring galaxies on the H I RC except when orientation and closeness of luminous galaxies produce a higher $|\vec{K} \bullet \vec{a}|$. Although the neighboring galaxy's effect is less significant on the RC, it does induce small perturbations in the orbits of particles that cause the observed asymmetry. Because the m_{s}/m_ι is smaller for higher metallicity particles, the effect of neighboring galaxies on the Hα RC is less.

Therefore, the finding of cluster effects on Hα RCs is subject to the sample selected and may be detected only when $|\vec{K} \bullet \vec{a}|$ is large

A large $|\vec{K} \bullet \vec{a}|$ requires the host galaxy be oriented appropriately and requires large $\vec{\nabla}\rho$. A large $\vec{\nabla}\rho$ is present near the cluster center or where the near galaxies are large and asymmetrically arranged around the host galaxy. The former condition is caused by the $\eta < 0$ of the galaxies in the cluster center surrounded by $\epsilon > 0$ of the galaxies in the cluster shell. Therefore, the SPM is consistent with the finding of Dale et al. (2001). The latter condition may be caused by a large, near neighbor galaxy.

The SPM's $(Gm_\mathrm{g} M_\mathrm{g} - G_\mathrm{s} m_\mathrm{s} L)/m_\iota R^2$ term has the form of a subtractive change in Newtonian acceleration. The SPM suggests the m_s change with radius causes the species of matter to change with radius that causes the appearance of a gravitational acceleration change with radius that is related to L. If the $|\vec{K} \bullet \vec{a}|$ term is small, the SPM effective force model reduces to the MOND model as was suggested in Hodge (2006) for elliptical galaxies.

The deviation of the data of NGC 5448 from Eq. (12) suggest a physical mechanism behind the quantized galaxy parameters. The clear departure from circular motion and the significant mass transfer inward ($\ddot{R} \neq 0$) found by Fathi et al. (2005) suggests this galaxy is in transition from one virial state to another. Further, the noted stellar and gas velocity difference decreases at larger radii. The better fitting of the $v^2_\mathrm{eormax} - L$ and of the $A_\mathrm{symax} - |\vec{K} \bullet \vec{a}_\mathrm{o}|$ relations is the expected result. NGC 3031 shows strong, non-circular motion in the disk (Gottesman et al., 1966). This suggests the integer variation is caused by the accumulation of mass at potential barriers such as at R_Δ and R_rrmax. Continued nucleosynthesis and changing $|\vec{K} \bullet \vec{a}_\mathrm{o}|$ causes an occasional, catastrophic rupture of one or more of the potential barriers, $\ddot{R} \neq 0$, and, therefore, the transition of the galaxy from one integer classification to another. A smoothly varying transition from the RR to the OR for flat or declining RCs such as NGC 4321 suggests mass is accumulating at a potential barrier at the end of the RR and is being depleted from the outer parts of the OR.

The proposition that observed asymmetries are caused by neighboring galaxies may also apply to bars and to the formation and maintenance of the rotation of mass around the galaxy.

Steinmetz & Navarro (2002) found in a series of N-body/gas dynamical simulations that included feedback: that feedback is a necessary component for morphology determination; that the main morphological component is regulated by the mode of gas accretion and intimately linked to *discrete* accretion events; that morphology is a transient phenomenon; and that the Hubble sequence reflects the varied accretion histories of galaxies. If luminosity is proportional to the ϵ, which directly causes the parameters of the RC, then there must exist a feedback mechanism controlling the parameters of the RC.

Approximately 66% of the sample galaxies have $a_1 = 4$ or $a_1 = 5$ as seen in Fig. 3 and Table 3. If $a_1 = 4.5$ is used in Eq. (12), $v^2_\mathrm{rrmax} \propto L$ for a majority of sample galaxies. Only NGC 4258 of the select galaxies would appear to be an outlier, which may suggest the v_rrmax is larger than the measured point chosen herein. Further, the neighboring galaxy effect would fail to improve the $v^2_\mathrm{rrmax} \propto L$ relation. The effect of the integer values is to broaden the applicability of the parameter $- L$ relations and to establish relations wherein the neighboring galaxy effect improves the calculation.

The SPM does not use the mass-to-light ratio to fit RCs. Indeed, Eqs. (14) and (19) imply the effective mass-to-light ratio varies among galaxies as observed.

The use of the M_B derived from the TF and the degree of correlation achieved herein suggests the mass term is totally determined by baryonic matter. The $\vec{\nabla}\rho$ field serves the same role in the equations as DM. Equation (3) with the L term and Eq. (7) with the M_Δ term suggests a much larger spiral galaxy baryonic mass [M of Eq. (3)] than traditional Newtonian mechanics calculates(Rv^2/G). Therefore, the $\vec{\nabla}\rho$ field causes Newtonian kinematic measurements to considerably underestimate mass in a galaxy ($M \approx Rv^2/G + G_\mathrm{s} m_\mathrm{s} L/G m_\iota$). The difference between the SPM and other RC models of the "missing mass problem" is that the added mass follows the luminous mass as suggested by the m_s/m_ι in the equations. Therefore, the added mass is baryonic rather than DM, a changing gravitation constant, a changing acceleration, or other form of "fifth force". The "missing mass" is non-luminous, baryonic matter.

The purpose of the present investigation was to expand the SPM to be consistent with galaxy RC, asymmetry and EOR observations. The resulting model adds the force of a scalar potential of the sample galaxy and of neighboring galaxies to the Newtonian rotation velocity equation. The form of the equation for each parameter of each region is the same with differing constants. Integer values, rather than scale factors, determine the particular galaxy parameter values. Among the sample galaxies, the B band luminosity of a galaxy is related (1) to the maximum rotation velocity, radius, mass, and acceleration parameters at the end of the RR and at the end of the EOR and (2) to the slope of the RC in the RR and OR. The scalar potential effect of the neighboring galaxies is related to the slope of the H I RC in the EOR, to the asymmetry in the OR, and to the residual of the measured and calculated values of the above mentioned luminosity dependent parameters. The RC in the OR may be rising, flat, or declining depending on the galaxy and its environment. The scalar potential field causes Newtonian mechanics to considerably underestimate the mass in galaxies. The Source of the scalar field appears as a monopole at distances of a few kpc from the center of spiral galaxies. The resulting RC equation is consistent with the formation, evolution, and long term maintenance of asymmetry observations. The RC observations are consistent with the SPM.

Acknowledgments

This research has made use of the NASA/IPAC Extragalactic Database (NED) which is operated by the Jet Propulsion Laboratory, California Institute of Technology, under contract with the National Aeronautics and Space Administration.

This research has made use of the LEDA database (http://leda.univ-lyon1.fr).

I thank those people who have commented on certain aspects of this paper that needed clarification.

I acknowledge and appreciate the financial support of Maynard Clark, Apollo Beach, Florida, while I was working on this project.

A The many lines in the parameter relations are not random.

The many lines in the plot in Fig. 3 suggest the data points may be random. The null hypothesis tested was "the data points are indeed random points". This null hypothesis was tested by following the procedure used in discovering Eq. (12) as follows: (1) A trial consisted of generating 15 sets of two random numbers between zero and one and subjecting the sets to the slope, correlation coefficient, and σ_e tests the galaxy sample passed. Call the independent variable (X_i) and the dependant variable (Y_i), where i varies from one to 15. (2) The equation tested was

$$Y_{\mathrm{calc}i} = K_1\, B^{t_i}\, X_i\,, \tag{39}$$

where K_1 is the proportionality constant, B is the exponential base determined by the relation to be tested, and t_i is the integer classification for the i^{th} set. (3) The K_1 value for each trial was calculated as the minimum value of $K_1 = Y_i/(B\,X_i)$ with an $X_i > 0.4$. (4) The t_i value was calculated for each set of (X_i, Y_i) values as

$$t_i = \text{ROUND}\left[\log_B\left(\frac{Y_i}{k_1\,X_i}\right)\right] , \tag{40}$$

where "ROUND" means to round the value in the braces to the nearest integer. (5) If any subset lacked a value, that subset was ignored. (6) If the correlation coefficient of any t_i subset of (X_i, Y_i) values, including the $(X_0, Y_0) = (0{,}0)$ point, was less than 0.90, the trial failed. (7) The $Y_{\text{calc}i}$ was calculated according to Eq. (39). If the $\sigma_{\text{e}} > 0.21$ between the Y_i and $Y_{\text{calc}i}$ for the 15 sets, the trail failed. (8) A count of the number N_π of sets of (X_i, Y_i) with $X_i^2 + Y_i^2 \leq 1$ and the number N_{XltY} of sets of (X_i, Y_i) with $X_i < Y_i$ was made. (9) The trial was redone with another 15 sets of random numbers for 30,000 trials.

For $B = 2$ the results were: (1) The $N_\pi/(15 \times 30,000) = 0.78528 \approx \pi/4$ and $N_{\text{XltY}}/(15 \times 30,000) = 0.49999$. Therefore, the random number generator performed satisfactorily. (2) Of the 30,000 trials 22 passed (0.07%), the remainder of the trials failed. Therefore, the null hypothesis was rejected with a 99+% confidence. For $B = 1.65$ the confidence level of rejecting the null hypothesis was greater than 0.95.

References

Aaronson M., Huchra J., Mould J., Schechter P. L., Tully R. B., 1982, ApJ, 258, 64

Baes M., Buyle P., Hau G. K. T., Dejonghe H., 2003, MNRAS, 341, L44

Battaner E., Florido E., 2000, Fundamentals of Cosmic Physics, 21, 1

Begeman K. G., Broeils A. H., Sanders R. H., 1991, MNRAS, 249, 523

Bekenstein J. D., 2004, Phys. Rev D, 70, 083509

Bertolami O., Páramos J., 2005, Phys. Rev D, 71, 023521

Binney J., Merrifield M., 1998, Galactic Astronomy. Princeton, NJ: Princeton University Press

Bosma A., 1981, AJ, 86, 1791

Bosma A., Goss W. M., Allen R. J., 1981, A&A, 93, 106

Bottema R., Pestaña J. L. G., Rothberg B., Sanders R. H., 2002, A&A, 393, 453

Braine J., Combes F., van Driel W., 1993, A&A, 280, 451

Broeils A. H., 1992, A&A, 256, 19

Brownstein J. R., Moffat J. W., 2006, ApJ, 636, 721

Carignan C., Freeman K. C., 1985, ApJ, 294, 494

Catinella B., Giovanelli R., Haynes M. P., 2006, ApJ, 640, 751

Ceccarelli M. L., Valotto C., Lambas D. G., Padilla N., Giovanelli R., Haynes M., 2005, ApJ, 622, 853

Chincarini G., de Souza R., 1985, A&A, 153, 218

Corbelli E., Salucci P., 2000, MNRAS, 311, 441

Courteau S., 1997, AJ, 114, 2402

Dale D. A., Giovanelli R., Haynes M. P., Hardy E., Campusano L. E., 2001, AJ, 121, 1886

Fathi K., van de Ven G., Peletier R. F., Emsellem E., Falcón-Barroso J., Cappellari M., de Zeeuw T., 2005, MNRAS, 364, 773

Fay S., 2004, A&A, 413, 799

Ferrarese L., 2002, ApJ, 578, 90

Ferrarese L., Merritt D., , 2002, Supermassive Black Holes

Fillmore J. A., Boroson T. A., Dressler A., 1986, ApJ, 302, 208

Freedman W. L., Madore B. F., Gibson B. K., Ferrarese L., Kelson D. D., Sakai S., Mould J. R., Kennicutt Jr. R. C., Ford H. C., Graham J. A., Huchra J. P., Hughes S. M. G., Illingworth G. D., Macri L. M., Stetson P. B., 2001, ApJ, 553, 47

García-Ruiz I., Sancisi R., Kuijken K., 2002, A&A, 394, 769

Garrido O., Marcelin M., Amram P., 2004, MNRAS, 349, 225

Ghez A. M., Morris M., Becklin E. E., Tanner A., Kremenek T., 2000, Nature, 407, 349

Goodman J., 2000, New Astronomy, 5, 103

Gottesman S. T., Davies R. D., Reddish V. C., 1966, MNRAS, 133, 359

Guhathakurta P., van Gorkom J. H., Kotanyi C. G., Balkowski C., 1988, AJ, 96, 851

Hodge J. C., 2006, New Astronomy, 11, 344

Hu F. X., Wu G. X., Song G. X., Yuan Q. R., Okamura S., 2006, Ap&SS, 302, 43

Huchtmeier W. K., 1975, A&A, 45, 259

Hudson M. J., Smith R. J., Lucey J. R., Branchini E., 2004, MNRAS, 352, 61

Jog C. J., 1997, ApJ, 488, 642

Jog C. J., 2002, A&A, 391, 471

Knapen J. H., Cepa J., Beckman J. E., Soledad del Rio M., Pedlar A., 1993, ApJ, 416, 563

Kornreich D. A., Haynes M. P., Jore K. P., Lovelace R. V. E., 2001, AJ, 121, 1358

Kornreich D. A., Haynes M. P., Lovelace R. V. E., van Zee L., 2000, AJ, 120, 139

Krumm N., Salpeter E. E., 1979, AJ, 84, 1138

Lilje P. B., Yahil A., Jones B. J. T., 1986, ApJ, 307, 91

Liszt H. S., Dickey J. M., 1995, AJ, 110, 998

Macri L. M., Stetson P. B., Bothun G. D., Freedman W. L., Garnavich P. M., Jha S., Madore B. F., Richmond M. W., 2001, ApJ, 559, 243

Mannheim P. D., Kmetko J., , 1996, Linear potentials and galactic rotation curves - detailed fitting

Mbelek J. P., 2004, A&A, 424, 761

McGaugh S., 1999, in Merritt D. R., Valluri M., Sellwood J. A., eds, ASP Conf. Ser. 182: Galaxy Dynamics - A Rutgers Symposium How Galaxies Don't Form: The Effective Force Law in Disk Galaxies. pp 528–+

Merritt D., Ferrarese L., 2002, in Knapen J. H., Beckman J. E., Shlosman I., Mahoney T. J., eds, The Central Kpc of Starbursts and AGNs Relationship of black holes to bulges

Moffat J. W., 2005, Journal of Cosmology and Astro-Particle Physics, 5, 3

Moore E. M., Gottesman S. T., 1998, MNRAS, 294, 353

Narlikar J. V., 2002, An Introduction to Cosmology. Cambridge, UK: Cambridge University Press

Padmanabhan T., Choudhury T. R., 2002, Phys. Rev D, 66, 081301

Pereira M. J., Kuhn J. R., 2005, ApJl, 627, L21

Persic M., Salucci P., Stel F., 1996, MNRAS, 281, 27

Pizzella A., Corsini E. M., Dalla Bontà E., Sarzi M., Coccato L., Bertola F., 2005, ApJ, 631, 785

Rejkuba M., 2004, A&A, 413, 903

Roscoe D. F., 2002, A&A, 385, 431

Rots A. H., 1975, A&A, 45, 43

Rubin V. C., Burstein D., Ford Jr. W. K., Thonnard N., 1985, ApJ, 289, 81

Sanders R. H., 2006, in Mamon G. A., Combes F., Deffayet C., Fort B., eds, EAS Publications Series MOND and Cosmology. pp 231–238

Sanders R. H., McGaugh S. S., 2002, ARA&A, 40, 263

Schödel R., et al., 2002, Nature, 419, 694

Sempere M. J., Garcia-Burillo S., Combes F., Knapen J. H., 1995, A&A, 296, 45

Shane W. W., Bieger-Smith G. P., 1966, Bull. Astron. Inst. Neatherlands, 18, 263

Sofue Y., Rubin V., 2001, ARA&A, 39, 137

Sofue Y., Tutui Y., Honma M., Tomita A., Takamiya T., Koda J., Takeda Y., 1999, ApJ, 523, 136

Steinmetz M., Navarro J. F., 2002, New Astronomy, 7, 155

Swaters R. A., Schoenmakers R. H. M., Sancisi R., van Albada T. S., 1999, MNRAS, 304, 330

Tadross A. L., 2003, New Astronomy, 8, 737

Takamiya T., Sofue Y., 2000, ApJ, 534, 670

Trujillo I., Carretero C., Patiri S. G., 2006, ApJl, 640, L111

Tully R. B., Fisher J. R., 1977, A&A, 54, 661

van Albada G. D., Shane W. W., 1975, A&A, 42, 433

van Albada T. S., Bahcall J. N., Begeman K., Sancisi R., 1985, ApJ, 295, 305

Vollmer B., Cayatte V., Boselli A., Balkowski C., Duschl W. J., 1999, A&A, 349, 411

Weinberg M. D., 1995, ApJl, 455, L31+

Whitmore B. C., Forbes D. A., Rubin V. C., 1988, ApJ, 333, 542

Will C., 1993, Theory and Experiment in Gravitational Physics. Cambridge, United Kingdom: Cambridge University Press

Willick J. A., 1999, ApJ, 516, 47